Electron energization by parallel electric fields in poloidal standing waves

P.A. Damiano¹, E.-H. Kim², J.R. Johnson³, and P. Porazik⁴

¹Geophysical Institute, University of Alaska Fairbanks, Fairbanks, AK 99775

²Princeton Plasma Physics Laboratory, Princeton University, Princeton, NJ 08543

³Department of Engineering and Computer Science, Andrews University, Berrien Springs, Michigan

⁴Lawrence Livermore National Laboratory, Livermore, California

Key Points:

- Point 1: The first full flux tube kinetic simulations of electron energization in poloidal standing modes are presented.
- Point 2: Electron energization and wave energy dissipation is increased with electron temperature and azimuthal mode number.
 - Point 3: The mono-energetic nature of the electron energization is consistent with previously published results for toriodal standing modes.

Corresponding author: Peter Damiano, padamiano@alaska.edu

Abstract

A hybrid gyrofluid-kinetic electron model is adapted and used to simulate poloidal standing modes for different electron temperatures and azimuthal mode numbers. As in previous studies of toroidal standing modes, mirror force effects lead to increased parallel potential drops, monoenergetic electron energization and wave energy dissipation as the ambient electron temperature is increased. A similar trend is also observed when the electron temperature is held fixed and the azimuthal mode number increased - owing to the narrowing of the azimuthal flux tube width which necessitates more electron energization to carry the increased parallel current density. In both cases, the increase in electron energization eventually leads to more rapid decreases in the parallel current with time because of the dissipation of wave energy.

1 Introduction

Standing waves in the magnetosphere occur in both toroidal and poloidal polarizations (where the perpendicular electric field is in the radial and azimuthal direction respectively). Toroidal modes generally result from mode conversion from fast compressional modes [Chen and Hasegawa, 1974; Southwood, 1974], while the generation of poloidal modes are associated with wave-particle interactions in the inner magnetosphere [Southwood, 1976; Chen and Hasegawa, 1988]. Poloidal modes also exist with or without significant magnetic compressional components [e.g. Dai et al., 2015] and both limits have similar occurrence rates that increase during stormtime conditions. Although the two polarizations of the standing waves can have different driving mechanisms, these waves are generally neither purely toroidal nor poloidal, but a mixture. Additionally, dominantly poloidal modes can gradually evolve into dominantly toroidal modes due to phase mixing effects [Radoski, 1967; Mann and Wright, 1995; Mann et al., 1997; Leonovich and Mazur, 1998] and under certain conditions, poloidal modes may change polarization to toroidal as they propagate across magnetic shells [Leonovich and Mazur, 1993; Klimushkin et al., 2004].

In the auroral context, toroidal modes have been linked to the formation of some discrete auroral arcs [e.g Samson et al., 2003; Lotko et al., 1998] and previous kinetic simulations [Damiano and Wright, 2008; Damiano and Johnson, 2012] illustrate a monoenergetic energization (consistent with the nature of the observed auroral arcs) under the influence of the wave parallel electric field. In the inner magnetosphere, the dom-

inant azimuthal electric and magnetic fields (for poloidal and toroidal modes respectively) 47 are in the direction of the magnetospheric particle drift and electrons can be energized 48 by drift/drift-bounce resonance to very high energies [e.g. Elkington et al., 1999, 2003; Ozeke and Mann, 2008; Shprits et al., 2008] which leads to an inward radial diffusion af-50 ter multiple wave-particle interactions [e.g. Elkington et al., 2003; Shprits et al., 2008; Ozeke et al., 2012. Modes with high azimuthal wave numbers $(m \approx 40-120)$ cannot 52 exhibit resonance with the electron drift motion, but non-resonant interaction of elec-53 trons with the wave azimuthal electric field can also lead to rapid radial transport [Ukhorskiy et al., 2009. The acceleration of electrons under the influence of the azimuthal electric field however does not preclude the potential for electron energization in poloidal Alfvén 56 modes by the parallel electric fields inherent in the wave (as evident in the toroidal case). 57 For example, in the theory of kinetic ballooning modes [e.g. Cheng and Lui, 1998; Cheng, 2004, which have poloidal polarization and have been linked to observations of auroral beads [e.g. Donovan et al., 2006; Rae et al., 2009; Motoba et al., 2012], parallel electric fields lead to the acceleration of the electrons. In the MHD limit, these ballooning modes 61 have zero frequency so we expect there would be good correspondence between the nature of electron energization in the growth phase of a low frequency poloidal standing 63 wave and electron energization in a ballooning mode. We have therefore adapted the 2-D gyrofluid-kinetic electron model [Damiano et al., 2007; Damiano et al., 2015], previously used to consider toroidal standing [e.g Damiano and Wright, 2008; Damiano and Johnson, 2012 and propagating [Damiano et al., 2015; Damiano et al., 2016] modes to study electron energization by parallel electric fields in poloidal standing waves. While this study is interesting in itself, this work also serves as a stepping stone to a more complicated investigation of electron energization in ballooning modes to be conducted in 70 future. The remainder of the paper is divided into three sections. Section 2 presents an overview of the hybrid gyrofluid-kinetic electron model that will be used in the inves-72 tigation. Section 3 presents the simulation results while Section 4 draws conclusions based on this analysis. 74

2 Hybrid Model

76

77

78

The model used is a version of the 2-D hybrid gyrofluid-kinetic electron model in dipolar coordinates [Damiano et al., 2007; Damiano et al., 2015] modified for the inclusion of poloidal Alfvén modes, but for the moment neglecting coupling to the compres-

sional mode. The geometry is illustrated in Figure 1b and explicitly includes the field aligned direction (x_1) and the direction across L shells (x_2) . For consideration of the poloidal modes, the gyrofluid portion of the model incorporates the modified linearized radial momentum equation given by

$$\mu_o \rho_o \frac{\partial \tilde{u_2}}{\partial t} = \frac{B_o}{h_1 h_2} \left(\frac{\partial}{\partial x_1} \left(h_2 b_2 \right) \right), \tag{1}$$

where $\tilde{u}_2 = (1 - 1.25 \rho_i^2 \nabla_\perp^2) u_2$, ρ_i is the ion gyroradius, $x_1 = \cos \theta / r^2$, $x_2 = \sin^2 \theta / r$, $x_3 = \phi$, $h_1 = r^3/(1 + 3\cos^2 \theta)^{1/2}$, $h_2 = r^2/(\sin \theta (1 + 3\cos^2 \theta)^{1/2})$, $h_3 = r\sin \theta$ (where θ is the angle subtended from the z axis as illustrated in Figure 1) and ρ_o and B_o denote the background plasma density and magnetic field respectively. The modified fluid velocity \tilde{u}_2 is defined to include the original cold plasma fluid velocity as well as a gyroviscosity term resulting from an off-diagonal term in the divergence of the pressure tensor. The coefficient of $\rho_i^2 \nabla_\perp^2$ is obtained from a Padé approximation [Johnson and Cheng, 1997; Cheng and Johnson, 1999]). Equation 1 is coupled to the radial component of Faraday's law given by

$$\frac{\partial b_2}{\partial t} = \frac{1}{h_1 h_3} \left(-\frac{\partial}{\partial x_3} (h_1 E_1) + \frac{\partial}{\partial x_1} (h_3 E_3) \right) = \frac{1}{h_1 h_3} \left(m h_1 E_1 + \frac{\partial}{\partial x_1} (h_3 E_3) \right), \quad (2)$$

where m is the imposed azimuthal mode number (such that u_2 , b_2 , $E_3 \propto \sin(m\phi)$ and $E_1 = E_{||} \propto \cos(m\phi)$) and the azimuthal (where a Padé approximation has also been used to relate \tilde{u} and the $\vec{E} \times \vec{B}$ velocity)

$$E_3 = B_o(1 - \rho_i^2 \nabla_\perp^2) \tilde{u}_2 \tag{3}$$

and parallel Ohm's laws

$$-m^{2}\left(\frac{h_{2}}{h_{1}h_{3}} + \frac{1}{h_{1}\lambda_{e}^{2}}\right)h_{1}E_{1} = m\left(\frac{h_{2}}{h_{1}h_{3}}\frac{\partial}{\partial x_{1}}(h_{3}E_{3})\right)$$

$$+ e\mu_{o}\frac{\partial}{\partial x_{1}}\int v_{1}^{2}fd^{3}v$$

$$+ \mu_{o}\frac{e}{m_{e}}\frac{\partial B_{o}}{\partial x_{1}}\int \mu_{m}fd^{3}v$$

$$- 2\mu_{o}\frac{e}{m_{e}}\frac{\partial B_{o}}{\partial x_{1}}\int \frac{m_{e}v_{1}^{2}}{2B_{o}}fd^{3}v.$$

$$(4)$$

Here, $\mu_m = m_e v_\perp^2/(2B)$ is the electron magnetic moment, the second term on the right hand side is associated with the parallel gradient of the electron pressure while the third and fourth terms are associated with the magnetic mirror force incorporating the perpendicular and parallel electron pressures respectively. This equation was derived, as presented for the toroidal mode in *Damiano et al.* [2007], using Ampere's law, Faraday's law and the gyroaveraged Vlasov equation, with the exception that the azimuthal component of Faraday's law (E_3) was used in place of the radial component (E_2) in order to consider poloidal modes.

The model equations are solved using a predictor-corrector method and equation (4) provides an estimate of parallel electric field at the predictor step. In order to enforce quasineutrality, any residual $\nabla \cdot \vec{j}$, is corrected for using the auxilliary Poisson's equation

$$\epsilon_{o} \frac{\partial}{\partial t} \left(\frac{1}{h_{1}h_{2}h_{3}} (mh_{1}h_{2}E_{3c}) \right) = -\nabla \cdot \vec{j}$$

$$= \frac{-1}{h_{1}h_{2}h_{3}} \left(\frac{\partial}{\partial x_{1}} (h_{2}h_{3}j_{e}) + mh_{1}h_{2}j_{3} \right)$$
(5)

where $j_e = -e \int v_1 f d^3 v$ is the electron parallel current and E_{3c} is the correction to the perpendicular electric field. Equation (5) is derived by taking the divergence of the full Ampere's law and and noting that $\nabla \cdot \vec{E}_{||} \ll \nabla \cdot \vec{E}_{\perp}$ [e.g. Damiano et al., 2005]. The correction is then applied to $E_{||}$ by incorporating E_{3c} in the first term on the right-hand-side of equation (4) at the corrector step [e.g. Damiano et al., 2003; Damiano et al., 2007].

The guiding center equations are used to describe the parallel electron dynamics

$$m_e \frac{dv_1}{dt} = -eE_1 - \mu_m \frac{1}{h_1} \frac{\partial B_o}{\partial x_1} \tag{6}$$

$$h_1 \frac{dx_1}{dt} = v_1, (7)$$

where v_1 is the parallel electron velocity and $v_{\perp} = \sqrt{v_2^2 + v_3^2}$ is the gyrophase independent perpendicular velocity. The corresponding integral moments of the electron distribution functions in equations (4) and (5) are treated computationally as summations using standard Particle-In-Cell techniques [Damiano et al., 2007].

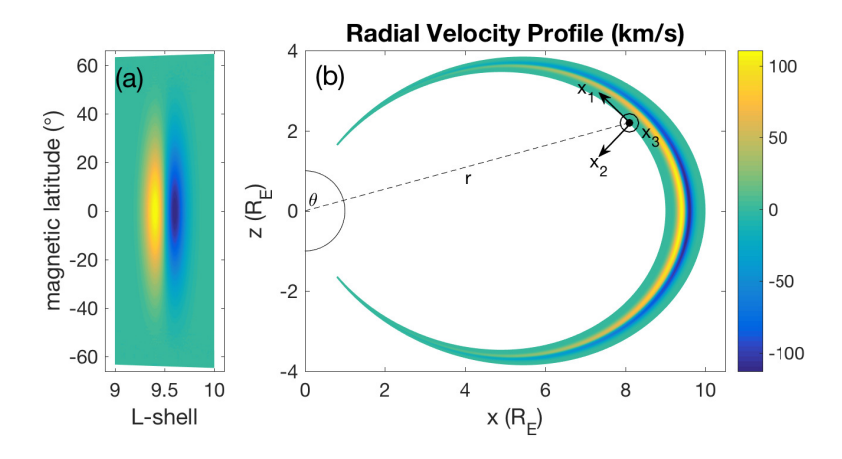


Figure 1. (a): Initial radial velocity perturbation (in km/s) presented as a function of magnetic latitude and L-shell. (b) Initial perturbation in cartesian coordinates. Inset displays the relation between polar and curvilinear coordinates where $x_1 = \cos \theta/r^2$, $x_2 = \sin^2 \theta/r$, $x_3 = \phi$ and θ is the angle subtended from the z-axis. The circle of radius 1 R_E denotes the surface of the Earth. The low altitude simulation boundary is at a geocentric distance of 2 R_E .

The neglect of the compressional mode, via the absence of the parallel magnetic field perturbation (b_1) , precludes coupling between the toroidal and poloidal Alfvén modes within the simulation and neglects electron energization associated with the parallel magnetic field perturbation [e.g. Klimushkin and Mager, 2014]. For the moment, the model is run independently for consideration of either toroidal or poloidal modes. As mentioned earlier, poloidal modes exist with or without significant compressional components [e.g. $Dai\ et\ al.$, 2015] and it is in limit of the latter (which are also generally high m modes) that this work most applies. However, it is our intention to generalize the model in future to include all three components of the magnetic field perturbation in tandem so that it is valid in high β plasmas where compressional effects are largest [e.g. Xia et al., 2017]. This inclusion is already done in our box model [Damiano et al., 2003]. Compressional modes have additionally been considered using both analytical gyrokinetic [Crabtree et al., 2003; Crabtree and Chen, 2004; Mager et al., 2013] and computational gyrokinetic [Porazik and Lin, 2011a,b] frameworks.

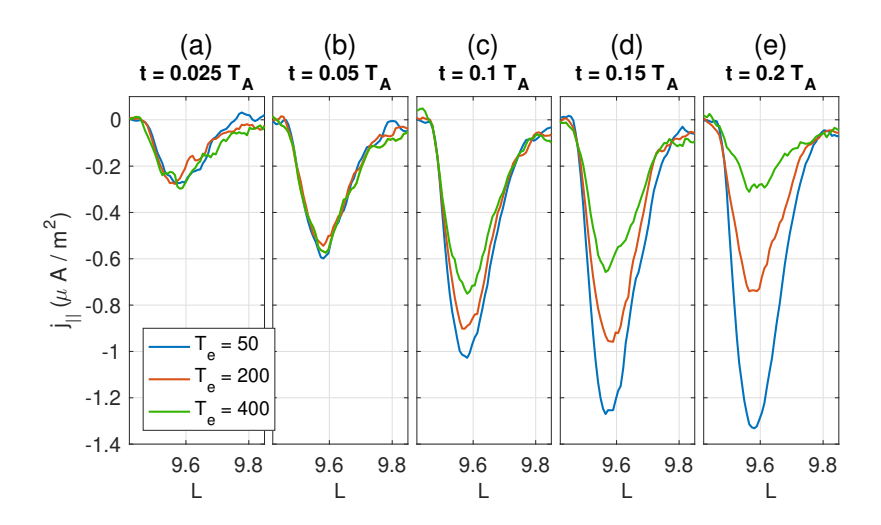


Figure 2. Parellel current evolution above the northern ionospheric boundary for m = 250 at the indicated times and temperatures.

3 Simulations

The simulation is initialized using an eigenmode solution for the velocity perturbation of a fundamental standing mode derived from the model of Taylor and Walker [1984]. The exact same functional dependence for the eigenmode as was used in previous studies [e.g. Damiano et al., 2007; Damiano and Wright, 2008; Damiano and Johnson, 2012] is used here except that we are initializing the radial (as opposed to azimuthal) velocity in order to drive the poloidal mode. The initial perturbation is displayed in Figure 1 and remains consistent for all the simulations presented. For the present study, we do not consider ion gyroradius effects (assuming $T_i = 0$ so that ρ_i corrections in \tilde{u}_2 and E_2 are neglected). This simplification is done for consistent comparison with our previously published works on toroidal standing modes and ρ_i effects will be addressed in a separate publication. In this paper, two limiting cases are considered.

3.1 Case of fixed azimuthal mode number and variable T_e

For the present section, we fix the azimuthal mode number to be m=250, but vary the electron temperature between 50 and 400 eV. Our choice of azimuthal wave number is admittedly high, but not unreasonable as cases of $m \sim 200$ have been inferred from observations [e.g. Takahashi et al., 2013] and high m modes do not generally have strong magnetic compressional components [e.g. Dai et al., 2015]. We also consider a large

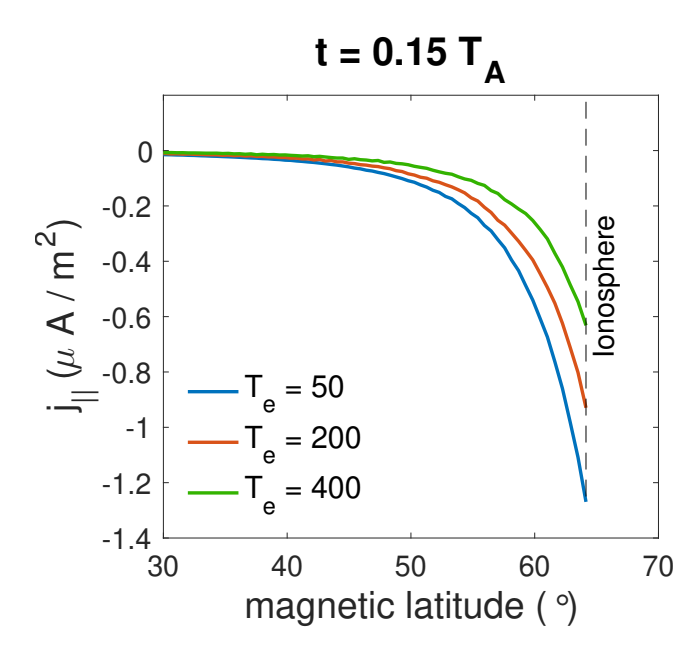


Figure 3. Parallel current density as a function of magnetic latitude along L=9.6? field line for indicated temperatures. In all cases, m=250.

range of m values here (more clearly evident in the next section) to emphasize trends. Figure 2 then illustrates the resulting profile of the parallel current for a cut along the northern low-altitude boundary (which is set at a geocentric distance of 2 R_E). Three different electron temperature cases are presented, and although the evolution looks quite similar at earlier times, there is a pronounced divergence as time increases. The amplitude of the higher temperature cases ($T_e = 200$ and 400 eV) begins to decrease after about t = 0.1-0.15 T_A while the the coldest temperature ($T_e = 50$ eV) case continues to grow, obtaining the largest amplitude.

Figure 3 then presents the field-aligned parallel current profile along L=9.6 and at t=0.15 T_A (same time as in Figure 2a). The increased current in all three temperature cases results from the converging magnetic field topology and the figure illustrates that the diverging current magnitudes evident in Figure 2 extend all along the field line. In order to understand these different parallel current magnitudes as a function of electron temperature, it is necessary to consider the evolution of the electron distribution in each of the cases. Figure 4 plots electron distribution functions at the northern low-altitude boundary in all the temperature cases. The distributions are taken along the field line of maximum parallel current (L=9.6) and are identical in feature to those generated for toroidal standing modes (and presented in Damiano and Wright [2008]).

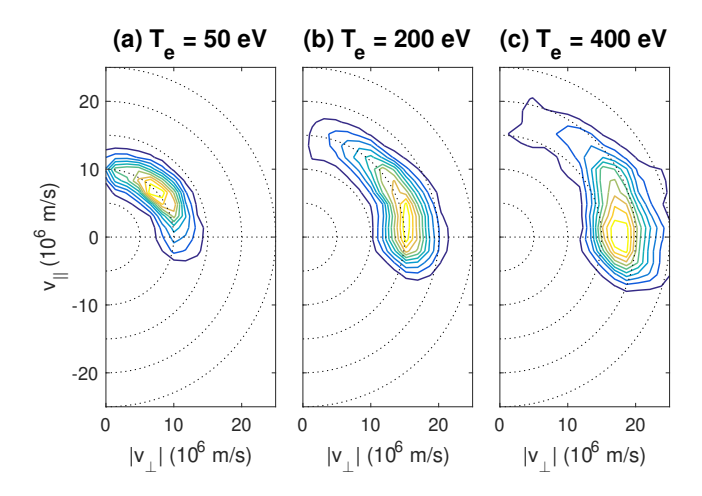


Figure 4. Distribution function at northern low-altitude boundary at $t = 0.15 T_A$ for (a) $T_e = 50 \text{ eV}$, (b) $T_e = 200 \text{ eV}$ and (c) $T_e = 400 \text{ eV}$.

The distributions are the result of the field-aligned acceleration of electrons (positive displacement to carry the negative field-aligned current) some of which then undergo reflection in the converging magnetic field topology and travel back up the field line forming the plotted ring distributions in velocity space. The radius of the ring is indicative of the magnitude of the parallel potential drop in the wave, which from a simple conservation of energy argument results as

$$e\Delta\phi = \frac{1}{2}m_e(v_{||}^2 + v_{\perp}^2).$$
 (8)

This relationship is what is expected to occur since the potential drop needed to overcome mirror force repulsion increases with the ambient electron temperature in the converging magnetic field topology [e.g. Knight, 1973; $Rankin\ et\ al.$, 1999; Nakamura, 2000; $Damiano\ and\ Wright$, 2008]. As more electrons are effectively trapped by the mirror force as temperature increases, fewer electrons must be accelerated to higher energies to carry a similar (or in this case) smaller parallel current. This point is illustrated in Figure 5 where the net energization of electrons at the northern low altitude boundary is presented as a function of time. The corresponding diminishment of the current can be understood by examining the profiles of the component energies in Figure 6. The drop in the energy in u_2 is indicative of ion drift energy being converted to both magnetic field and electron energy. The magnetic field energy (and correspondingly the magnitude of $j_{||}$) drops

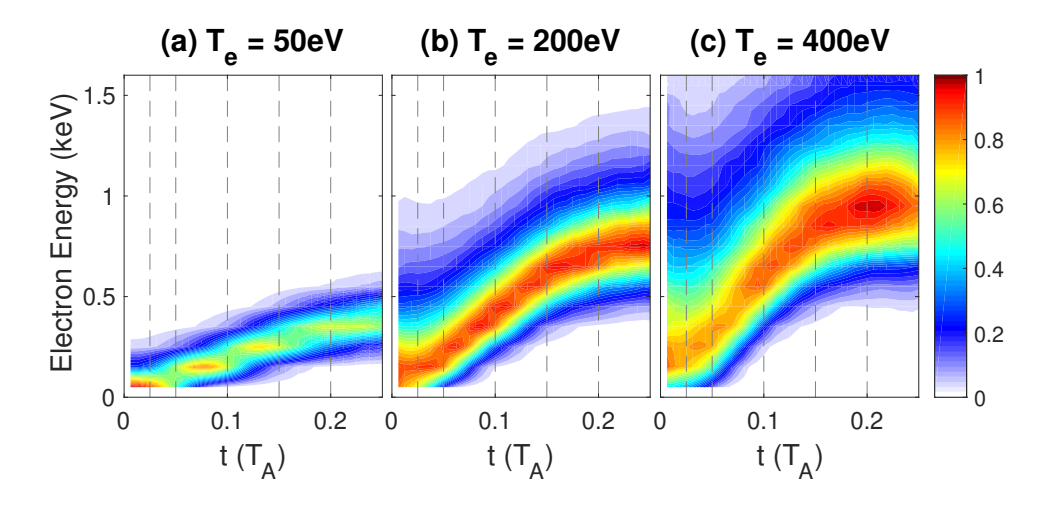


Figure 5. Energy of the accelerated electron population in the region of the current maximum as a function of time for (a) $T_e = 50$ eV, (b) $T_e = 200$ eV and (c) $T_e = 400$ eV. In all cases, the azimuthal mode number is 250.

as progressively more ion kinetic energy is transferred to electron energization to carry the parallel current as the electron temperature is increased.

As mentioned, the qualitative features of the electron energization presented in this section is very similar to that seen for toroidal modes. This similarity is to be expected since the change in wave polarization should not alter the characteristics of the electron energization which is defined by the mirror force topology rather than the polarization of the wave. The mirror force effect on $E_{||}$ in toroidal standing modes was first noted by $Rankin\ et\ al.\ [1999]$ (and subsequent publications $Tikhonchuk\ and\ Rankin\ [2000,\ 2002]$). Rather than in simulations as presented here, they considered the relation between $E_{||}$ and $j_{||}$ (in the quasi-static) via the evaluation of the non-local conductivity matrix derived from the low frequency electron gyrokinetic equation $[Antonsen\ and\ Lane,\ 1980]$ in a dipolar geometry. In the next section, we extend our consideration of the the poloidal wave system to the limit of fixed electron temperature and variable azimuthal mode number.

3.2 Case of fixed electron temperature $(T_e=200~{\rm eV})$ and variable m

In analogy to Figure 2, Figure 7 displays the parallel current density evolution at the northern ionospheric boundary for a fixed electron temperature, but for variable azimuthal mode number. Initially, the magnitude of the parallel current density increases

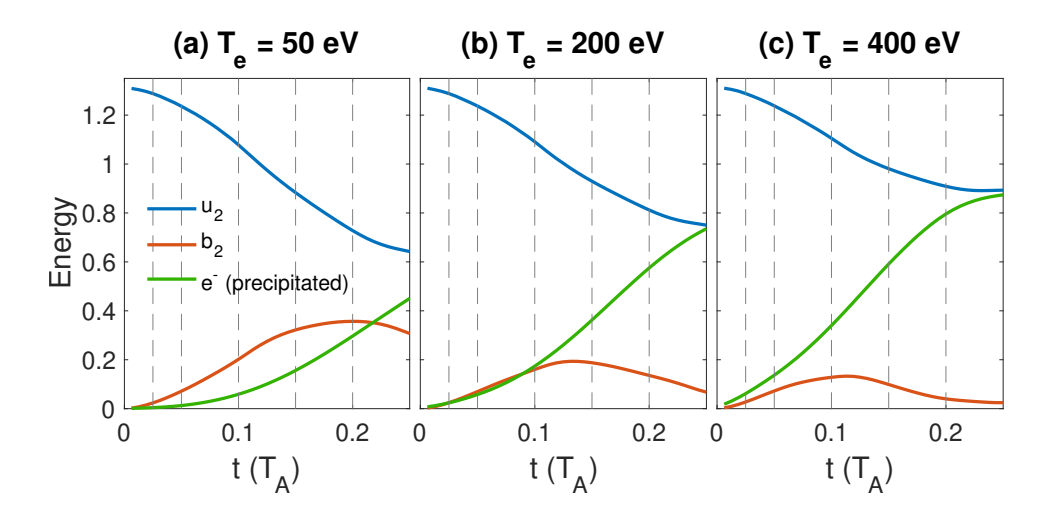


Figure 6. Component energies for (a) $T_e = 50 \text{ eV}$, (b) $T_e = 200 \text{ eV}$ and (c) $T_e = 400 \text{ eV}$. In all cases, the azimuthal mode number is 250.

with the azimuthal mode number (Figures 7a-7c). This trend is as would be expected because the flux tube width narrows as the azimuthal mode number is increased and the magnitude of j_1 must increase in order to carry the same total parallel current through a narrower channel. However, the increased parallel current density needs to be carried by more energetic electrons. Therefore, since the simulation is un-driven, the fixed initial wave energy is dissipated most quickly in the highest azimuthal mode number case (m = 250) meaning that the parallel current density begins to decrease relative to the lower m cases as time goes on (Figures 7d and 7e).

The increased energization of the electrons with the increase in m (and parallel current density) is illustrated in Figures 8 and 9. As per equation (8) the increased potential drop needed to accelerate electrons results in a larger radius in velocity space (Figure 8). Figure 9 then displays the partitioning of the wave energy for the three values of the azimuthal mode number considered. The initial ion kinetic energy is consistent in each case, but as m is increased, the energy transferred to the magnetic field goes down dramatically at the expense of wave energy going into the energization of precipitating electrons. This reduction in the magnetic field energy also accounts for the drop in parallel current density for the largest azimuthal mode number evident in Figures 7d and 7e. It should be noted that the total energy does not appear constant in Figure 9 because the analysis neglects the initial thermal energy of the electrons.

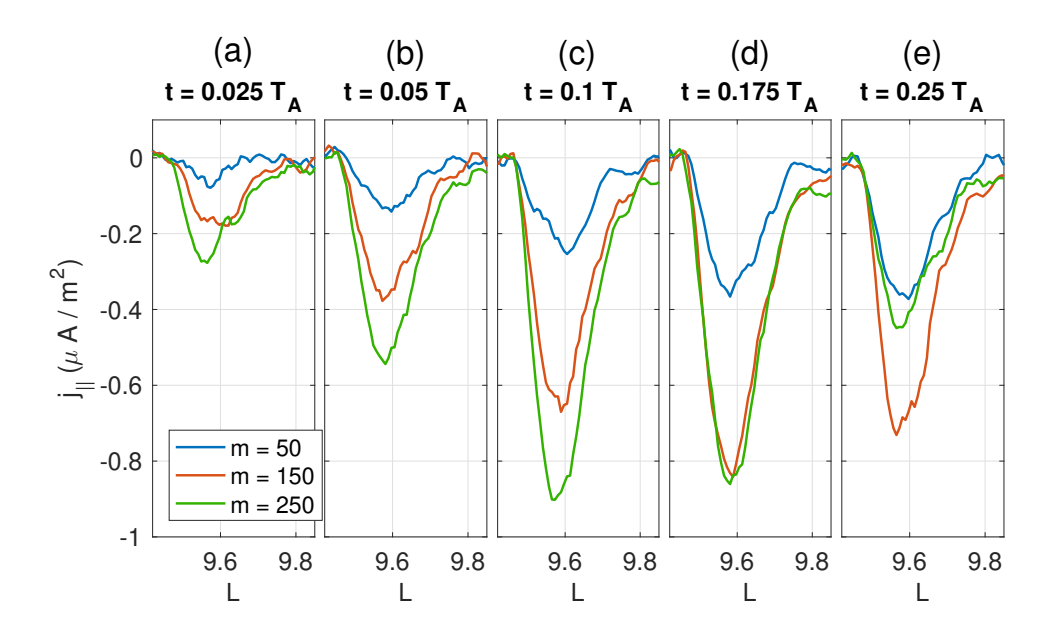


Figure 7. Parellel current evolution above the northern ionospheric boundary for $T_e = 200 \text{ eV}$ at the indicated times and m values.

228

240

241

242

243

244

245

246

247

248

249

250

251

252

253

254

255

As a final comment, it should be noted that there is one large difference between the poloidal standing mode simulations presented here and the toroidal mode studies done previously [Damiano et al., 2007; Damiano and Wright, 2008; Damiano and Johnson, 2012, 2013]. In these latter efforts, there was substantial broadening of the parallel current profile in the radial direction which was due to the perpendicular Poynting flux associated with the large parallel electric field $S_2 = -E_1b_3$ [e.g Damiano and Johnson, 2013] where b_3 is the azimuthal magnetic field perturbation associated with the toroidal standing mode. As apparent in Figures 2 and 7, there is no similar radial broadening in the poloidal examples presented here. This lack however is simply because the magnetic field perturbation associated with the poloidal mode is in the radial direction and the corresponding perpendicular Poynting flux would be in the azimuthal direction. This broadening is outside the remit of our present 2D model and will be addressed when we expand to consideration of 3D simulations. As in the 2D case though, the effect of the broadening would further decreases the amplitude of the parallel current and electron energization to what is apparent in these examples as more of the total parallel current is being carried along adjacent field lines.

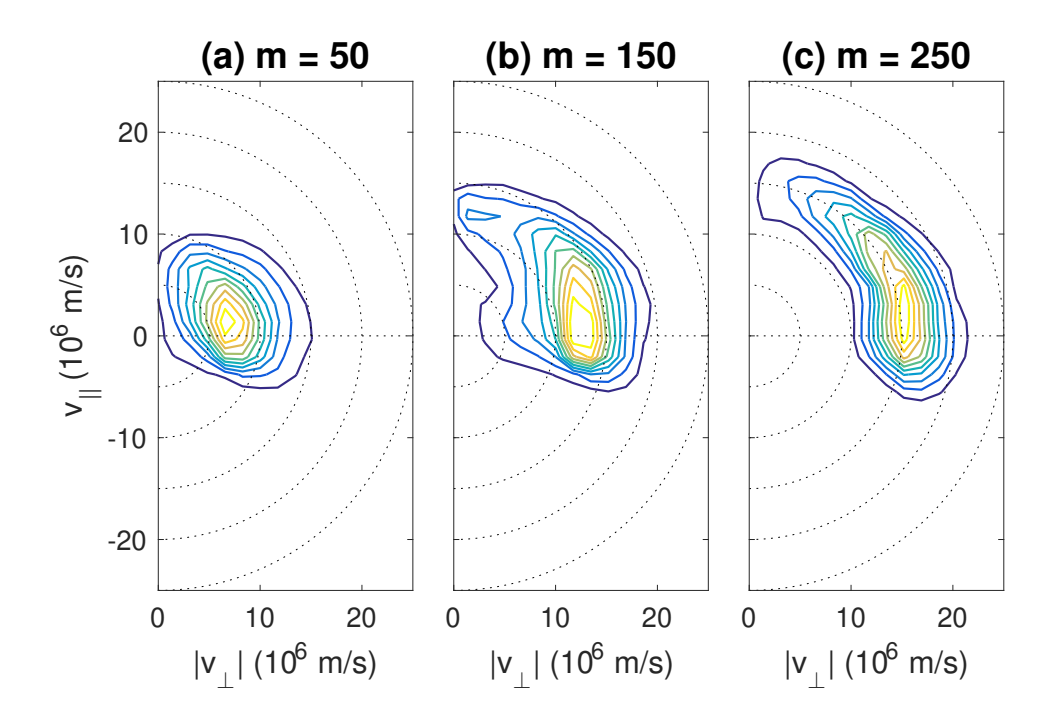


Figure 8. Distribution function at northern low-altitude boundary at $t = 0.15 T_A$ for (a) m = 50, (b) m = 150 and (c) m = 250.

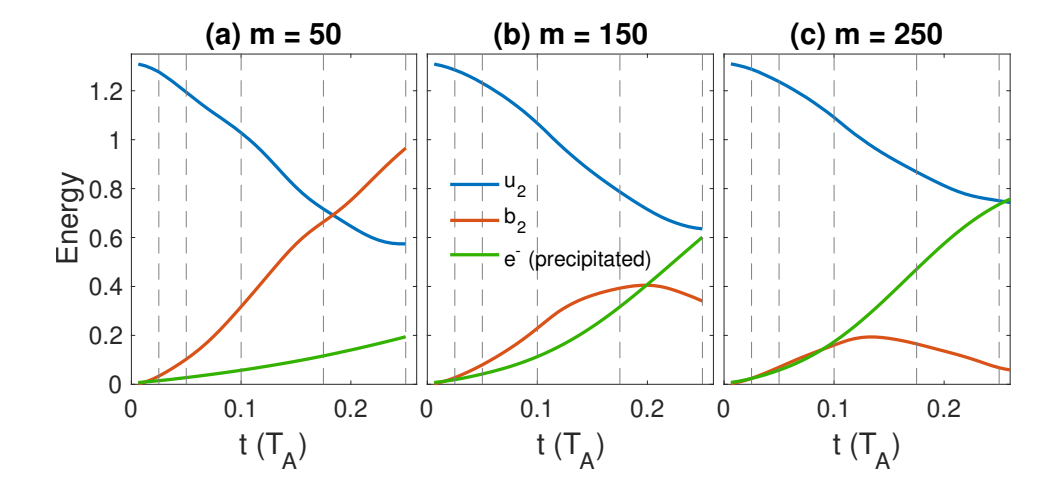


Figure 9. Component energies for (a) m = 50, (b) m = 150 eV and (c) m = 250 eV. In all cases, the electron temperature is 200 eV.

4 Conclusions

260

In this study, a 2D hybrid gyrofluid-kinetic electron model in dipolar coordinates 261 is used to study electron acceleration in the parallel electric fields of poloidal standing 262 modes in the Earth's magnetosphere. It was found that the electron energization increased 263 with increasing ambient electron temperature owing to mirror force trapping effects. It was found that, consistent with previous studies of toroidal standing modes, the elec-265 tron energization increased with increasing ambient electron temperature owing to mirror force effects. The resulting simulation energized electron populations formed ring dis-267 tributions in velocity space. While the electron energization increased, the net parallel current was seen to decrease because of the associated dissipation of wave energy. In the 269 limit of fixed electron temperature, but increasing azimuthal wave number, both the par-270 allel current and electron energization were seen to increase due to the narrowing of the 271 flux tube in the azimuthal direction. Over the longer term though, the magnitude of the 272 parallel current in the highest m case considered decreased significantly because of the 273 dissipation of wave energy inherent in the increased acceleration of the electrons that oc-274 curred at earlier times. 275

Acknowledgments

276

288

- This material is based upon work supported by the U.S. Department of Energy, Office
- of Science, Office of Fusion Energy Sciences under contract numbers DE-AC02-09CH11466.
- Work at Princeton University is under NASA grants NNH14AY20I, NNH15AB17I, 80HQTR18T0066,
- NNX17AI50G, NNH16AC43I and NSF grant AGS1602855. Work at the University of
- Alaska is under NASA grants 80NSSC18K0835 and NSF grant AGS1832207. Work at
- Andrews University is under NASA grants NNX17AI47G, NNX16AR10G, NNH15AB17I,
- ²⁸³ NNX16AQ87G, NNX17AI50G, 80NSSC18K0835 and NSF grant AGS1832207. This work
- was also supported in part by the high-performance computing and data storage resources
- operated by the Princeton Plasma Physics Laboratory and the Research Computing Sys-
- tems Group at the University of Alaska Fairbanks Geophysical Institute. The simula-
- tion data used in the figures may be accessed at https://github.com/padamiano/JGR2019data).

References

- Antonsen, T. M., Jr., and B. Lane (1980), Kinetic equations for low frequency
- instabilities in inhomogeneous plasmas, *Physics of Fluids*, 23, 1205–1214, doi:

- 291 10.1063/1.863121.
- Chen, L., and A. Hasegawa (1974), A theory of long-period magnetic pulsations: 1.
- Steady state excitation of field line resonance, J. Geophys. Res., 79, 1024–1032,
- doi:10.1029/JA079i007p01024.
- ²⁹⁵ Chen, L., and A. Hasegawa (1988), On magnetospheric hydromagnetic waves ex-
- cited by energetic ring-current particles, J. Geophys. Res., 93, 8763–8767, doi:
- ²⁹⁷ 10.1029/JA093iA08p08763.
- ²⁹⁸ Cheng, C. Z. (2004), Physics of Substorm Growth Phase, Onset, and Dipolarization,
- Space Science Reviews, 113, 207–270, doi:10.1023/B:SPAC.0000042943.59976.0e.
- Cheng, C. Z., and J. R. Johnson (1999), A kinetic-fluid model, J. Geophys. Res.,
- 104, 413–428, doi:10.1029/1998JA900065.
- Cheng, C. Z., and A. T. Y. Lui (1998), Kinetic ballooning instability for substorm
- onset and current disruption observed by AMPTE/CCE, Geophys. Res. Lett., 25,
- 4091-4094, doi:10.1029/1998GL900093.
- 205 Crabtree, C., and L. Chen (2004), Finite gyroradius theory of drift compressional
- modes, Geophys. Res. Lett., 31, L17804, doi:10.1029/2004GL020660.
- Crabtree, C., W. Horton, H. V. Wong, and J. W. van Dam (2003), Bounce-averaged
- stability of compressional modes in geotail flux tubes, Journal of Geophysical
- Research (Space Physics), 108, 1084, doi:10.1029/2002JA009555.
- Dai, L., K. Takahashi, R. Lysak, C. Wang, J. R. Wygant, C. Kletzing, J. Bonnell,
- C. A. Cattell, C. W. Smith, R. J. MacDowall, S. Thaller, A. Breneman, X. Tang,
- X. Tao, and L. Chen (2015), Storm time occurrence and spatial distribution of
- Pc4 poloidal ULF waves in the inner magnetosphere: A Van Allen Probes sta-
- tistical study, Journal of Geophysical Research (Space Physics), 120, 4748–4762,
- doi:10.1002/2015JA021134.
- Damiano, P. A., and J. R. Johnson (2012), Electron acceleration in a ge-
- omagnetic Field Line Resonance, Geophys. Res. Lett., 39, L02102, doi:
- 10.1029/2011GL050264.
- Damiano, P. A., and J. R. Johnson (2013), Mirror force induced wave dispersion in
- Alfvén waves, *Physics of Plasmas*, 20(6), 062,901, doi:10.1063/1.4810788.
- Damiano, P. A., and A. N. Wright (2008), Electron thermal effects in standing shear
- Alfvén waves, Journal of Geophysical Research (Space Physics), 113, A09219,
- doi:10.1029/2008JA013087.

- Damiano, P. A., R. D. Sydora, and J. C. Samson (2003), Hybrid
- magnetohydrodynamic-kinetic model of standing shear Alfvén waves, Journal
- of Plasma Physics, 69, 277–304, doi:10.1017/S0022377803002216.
- Damiano, P. A., A. N. Wright, R. D. Sydora, and J. C. Samson (2005), Hybrid
- magentohydrodynamic-kinetic electron closure methods and shear Alfvén waves in
- nonuniform plasmas, *Phys. Plasmas*, 12, 042,105.
- Damiano, P. A., A. N. Wright, R. D. Sydora, and J. C. Samson (2007), Energy dis-
- sipation via electron energization in standing shear Alfvén waves, *Phys. Plasmas*,
- 14, 062,904.
- Damiano, P. A., J. R. Johnson, and C. C. Chaston (2015), Ion temperature effects
- on magnetotail Alfvén wave propagation and electron energization, Journal of
- 335 Geophysical Research (Space Physics), 120, 5623–5632, doi:10.1002/2015JA021074.
- Damiano, P. A., J. R. Johnson, and C. C. Chaston (2016), Ion gyroradius effects
- on particle trapping in kinetic Alfvén waves along auroral field lines, Journal of
- 338 Geophysical Research (Space Physics), 121, 10, doi:10.1002/2016JA022566.
- Donovan, E., S. Mende, B. Jackel, H. Frey, M. Syrjäsuo, I. Voronkov, T. Trondsen,
- L. Peticolas, V. Angelopoulos, S. Harris, M. Greffen, and M. Connors (2006), The
- THEMIS all-sky imaging array system design and initial results from the proto-
- type imager, Journal of Atmospheric and Solar-Terrestrial Physics, 68(13), 1472 –
- 343 1487.
- Elkington, S. R., M. K. Hudson, and A. A. Chan (1999), Acceleration of relativistic
- electrons via drift-resonant interaction with toroidal-mode Pc-5 ULF oscillations,
- 346 Geophys. Res. Lett., 26, 3273–3276, doi:10.1029/1999GL003659.
- Elkington, S. R., M. K. Hudson, and A. A. Chan (2003), Resonant acceleration and
- diffusion of outer zone electrons in an asymmetric geomagnetic field, Journal of
- 349 Geophysical Research (Space Physics), 108, 1116, doi:10.1029/2001JA009202.
- Johnson, J. R., and C. Z. Cheng (1997), Kinetic Alfvén waves and plasma transport
- at the magnetopause, Geophys. Res. Lett., 24, 1423–1426, doi:10.1029/97GL01333.
- Klimushkin, D., P. Mager, and K. Glassmeier (2004), Toroidal and poloidal Alfvén
- waves with arbitrary azimuthal wavenumbers in a finite pressure plasma in the
- Earth's magnetosphere, Annales Geophysicae, 22, 267–287, doi:10.5194/angeo-22-
- ³⁵⁵ 267-2004.

- Klimushkin, D. Y., and P. N. Mager (2014), The Alfvén wave parallel electric field
- in non-uniform space plasmas, Astronomy and Space Science, 350, 579–583, doi:
- 10.1007/s10509-013-1774-x.
- Knight, S. (1973), Parallel electric fields, Planet. Space Sci., 21, 741.
- Leonovich, A. S., and V. A. Mazur (1993), A theory of transverse small-scale stand-
- ing Alfven waves in an axially symmetric magnetosphere, Planet. Space Sci., 41,
- 362 697–717, doi:10.1016/0032-0633(93)90055-7.
- Leonovich, A. S., and V. A. Mazur (1998), Standing Alfvén waves with $m \gg 1$
- in an axisymmetric magnetosphere excited by a non-stationary source, Annales
- 365 Geophysicae, 16, 914–920, doi:10.1007/s00585-998-0914-z.
- Lotko, W., A. V. Streltsov, and C. W. Carlson (1998), Discrete auroral arc, elec-
- trostatic shock and suprathermal electrons powered by dispersive, anonamously
- resistive field line resonance, Geophys. Res. Lett., 25, 4449.
- Mager, P. N., D. Y. Klimushkin, and D. V. Kostarev (2013), Drift-compressional
- modes generated by inverted plasma distributions in the magnetosphere, Journal
- of Geophysical Research (Space Physics), 118, 4915–4923, doi:10.1002/jgra.50471.
- Mann, I. R., and A. N. Wright (1995), Finite lifetimes of ideal poloidal Alfvén
- waves, J. Geophys. Res., 100, 23,677–23,686, doi:10.1029/95JA02689.
- Mann, I. R., A. N. Wright, and A. W. Hood (1997), Phase-mixing poloidal alfvén
- wave polarisations, Advances in Space Research, 20, 489–492, doi:10.1016/S0273-
- 1177(97)00716-3.
- Motoba, T., K. Hosokawa, A. Kadokura, and N. Sato (2012), Magnetic conjugacy
- of northern and southern auroral beads, Geophys. Res. Lett., 39, L08108, doi:
- 10.1029/2012GL051599.
- Nakamura, T. K. (2000), Parallel electric field of a mirror kinetic Alfvén wave, J.
- Geophys. Res., 105, 10,729-10,738, doi:10.1029/1999JA900494.
- Ozeke, L. G., and I. R. Mann (2008), Energization of radiation belt electrons by ring
- current ion driven ULF waves, Journal of Geophysical Research (Space Physics),
- 384 113, A02201, doi:10.1029/2007JA012468.
- Ozeke, L. G., I. R. Mann, K. R. Murphy, I. J. Rae, D. K. Milling, S. R. Elkington,
- A. A. Chan, and H. J. Singer (2012), ULF wave derived radiation belt radial dif-
- fusion coefficients, Journal of Geophysical Research (Space Physics), 117, A04222,
- doi:10.1029/2011JA017463.

- Porazik, P., and Z. Lin (2011a), Gyrokinetic Simulation of Magnetic Compressional
- Modes in General Geometry, Communications in Computational Physics, 10,
- 899–911, doi:10.4208/cicp.241110.280111a.
- Porazik, P., and Z. Lin (2011b), Gyrokinetic particle simulation of drift-
- compressional modes in dipole geometry, *Physics of Plasmas*, 18(7), 072107,
- doi:10.1063/1.3605031.
- Radoski, H. R. (1967), Highly asymmetric MHD resonances: The guided poloidal
- mode, J. Geophys. Res., 72, 4026–4027, doi:10.1029/JZ072i015p04026.
- Rae, I., I. Mann, K. Murphy, D. Milling, A. Parent, V. Angelopoulos, H. Frey,
- A. Kale, C. Watt, S. Mende, and C. Russell (2009), Timing and localization of
- ionospheric signatures associated with substorm expansion phase onset, Journal of
- Geophysical Research (Space Physics), 114 (A13), A00C09.
- Rankin, R., J. C. Samson, and V. T. Tikhonchuk (1999), Parallel electric fields in
- dispersive shear Alfvén waves in the dipolar magnetosphere, Geophys. Res. Lett.,
- 26, 3601–3604, doi:10.1029/1999GL010715.
- Samson, J. C., R. Rankin, and V. T. Tikhonchuk (2003), Optical signatures of auro-
- ral arcs produced by field line resonances: Comparison with satellite observations
- and modeling, Ann. Geophys., 21, 933.
- Shprits, Y. Y., S. R. Elkington, N. P. Meredith, and D. A. Subbotin (2008), Review
- of modeling of losses and sources of relativistic electrons in the outer radiation
- belt I: Radial transport, Journal of Atmospheric and Solar-Terrestrial Physics, 70,
- 410 1679–1693, doi:10.1016/j.jastp.2008.06.008.
- Southwood, D. J. (1974), Some features of field line resonances in the magneto-
- sphere, Planet. Space Sci., 22, 483–491, doi:10.1016/0032-0633(74)90078-6.
- Southwood, D. J. (1976), A general approach to low-frequency instability in the ring
- current plasma, J. Geophys. Res., 81, 3340–3348, doi:10.1029/JA081i019p03340.
- Takahashi, K., M. D. Hartinger, V. Angelopoulos, K.-H. Glassmeier, and H. J.
- Singer (2013), Multispacecraft observations of fundamental poloidal waves without
- ground magnetic signatures, Journal of Geophysical Research (Space Physics),
- 418 118, 4319–4334, doi:10.1002/jgra.50405.
- Taylor, J. P. H., and A. D. M. Walker (1984), Accurate approximate formulae
- for toroidal standing hydromagnetic oscillations in a dipolar geomagnetic field,
- Planet. Space Sci., 32, 1119–1124, doi:10.1016/0032-0633(84)90138-7.

- Tikhonchuk, V. T., and R. Rankin (2000), Electron kinetic effects in standing shear
- Alfvén waves in the dipolar magnetosphere, *Physics of Plasmas*, 7, 2630–2645,
- doi:10.1063/1.874105.
- Tikhonchuk, V. T., and R. Rankin (2002), Parallel potential driven by a kinetic
- Alfvén wave on geomagnetic field lines, Journal of Geophysical Research (Space
- Physics), 107, 1104, doi:10.1029/2001JA000231.
- Ukhorskiy, A. Y., M. I. Sitnov, K. Takahashi, and B. J. Anderson (2009), Radial
- transport of radiation belt electrons due to stormtime Pc5 waves, Annales Geo-
- physicae, 27, 2173–2181, doi:10.5194/angeo-27-2173-2009.
- Xia, Z., L. Chen, L. Zheng, and A. A. Chan (2017), Eigenmode analysis of compres-
- sional poloidal modes in a self-consistent magnetic field, Journal of Geophysical
- Research (Space Physics), 122, 10, doi:10.1002/2017JA024376.